

# Towards a non-invasive diagnosis of portal hypertension based on an Eulerian CFD model with diffuse boundary conditions

Lixin Ren<sup>1,3</sup>, Shang Wan<sup>2</sup>, Yi Wei<sup>2</sup>, Xiaowei He<sup>1,3</sup>(✉),  
Bin Song<sup>2</sup>(✉), and Enhua Wu<sup>1,4</sup>

<sup>1</sup> SKLCS, Institute of Software, Chinese Academy of Sciences, Beijing, China  
xiaowei@iscas.ac.cn

<sup>2</sup> Dpt. of Radiology, West China Hospital, Sichuan University, Chengdu, China  
songlab\_radiology@163.com

<sup>3</sup> University of Chinese Academy of Sciences, Beijing, China

<sup>4</sup> Faculty of Science and Technology, University of Macau, Macao, China

**Abstract.** Portal hypertension is one of the major complications in patients with chronic liver diseases (CLD) which induces the increase in portal vein gradient pressure. At advanced stage, it can cause the esophageal varices and variceal hemorrhage. Therefore, portal hypertension has been the leading cause of mortality in CLD patients. To diagnose portal hypertension, the invasive hepatic venous pressure gradient (HVPG) measurement is still the only validated technique to accurately evaluate changes in portal pressure and regarded as the standard reference. However, it entails the limitation of invasive procedure and have the risk of further bleeding and inflammation. In this paper we propose an Eulerian computational fluid dynamics (CFD) model to facilitate hemodynamics analysis. To enable consistent simulation results with different boundary conditions, a diffuse boundary handling technique was proposed to impose smooth boundary conditions for both the pressure and velocity fields. We also propose a computational workflow for quantifying patient-specific hemodynamics in portal vein systems non-invasively. The simulation is performed on patient-specific PV models reconstructed from CT angiographic images. Experiments show that pressure changes in the PV of patients with portal hypertension due to blockage of the RPV are significantly lower than that of normal subjects.

**Keywords:** Diffuse boundary conditions · Pressure change · Non-invasive diagnosis · Portal hypertension · CFD.

## 1 Introduction

Portal hypertension is the hemodynamics abnormality associated with the most severe complications of cirrhosis (including ascites, hepatic encephalopathy and

---

L.Ren and S.Wan-These authors contributed equally to this work.

bleeding from gastroesophageal varices), and has emerged as the leading cause of mortality in cirrhotic patients [3]. While liver cirrhosis arise from various causes including viruses, toxins, and genetics, a common theory indicates that portal hypertension mainly arise from the increased blood pressure in portal vein, possibly due to an increased resistance to blood flow through the portal system [15]. According to the anatomy, the portal vein system is joined by the superior mesenteric vein (SMV) and splenic vein (SV), and then divides into the left portal vein (LPV) and the right portal vein (RPV) branches which entering the left and right liver lobes, respectively [2]. At advanced stage of liver cirrhosis, patients with terminal hepatic failure (THF) were observed with atrophy in the right liver lobe while hypertrophy in the left liver lobe [17]. This phenomenon indicates the resistance to blood flow in the right portal vein may be increased, causing increased blood pressure in the veins of the portal system. However, the direct measurement of blood pressure inside the portal vein is difficult. The invasive hepatic venous pressure gradient (HVPG) measurement is still the only validated technique to accurately evaluate changes in portal pressure.

In recent years, computational fluid dynamics (CFD) has shown great potential in hemodynamic analysis, together with noninvasive and invasive imaging techniques [18]. Since CFD itself has a variety of different methods and each has its own advantages and shortcomings, it should be rather careful when adopting a numerical method to study the hepatic flow. For example, the accuracy of the finite element method (FEM) is largely influenced by the temporal/spatial resolutions, numerical solvers and boundary handling techniques [8]. In hemodynamics analysis, the choice of boundary conditions is in fact of particular importance to better reproduce *in vivo* conditions because only a small part of the PV system will be retained for simulation [11]. Despite the recognized importance [16, 5], previous works on how to find a CFD-based identifier that can help diagnose portal hypertension noninvasively are rather limited [14] and only a few studies have devoted efforts to addressing the intrinsic issues in computational models to better understanding hemodynamics in PV systems. Most of them only apply the FEM solver to solve hemodynamics in the PV system, yet pay no attention on the numerical problems [12].

In this paper, we propose an Eulerian CFD model to facilitate hemodynamics analysis. Our method is based on the assumption that the increased blood pressure in the portal vein system is caused by the blockage in the blood flow through the cirrhotic liver tissue. For patients with portal hypertension, the large veins are subsequently developed to get around the blockage. Therefore, if the same boundary conditions are applied and a blockage is applied on right portal vein, the pressure change in PV systems of patients with portal hypertension is expected to be smaller than those without portal hypertension. To verify this idea, the following contributions were made: (1) an Eulerian computational fluid dynamics model for quantifying patient-specific hemodynamics in portal vein systems; (2) a diffuse boundary handling technique that is able to impose smooth boundary conditions for both the pressure and velocity fields;

(3) a workflow for quantifying pressure changes in PV that helps discriminate patients with portal hypertension from normal subjects.

## 2 Methodology

### 2.1 Blood flow model

In 3D Eulerian space, the general model for the hemodynamics in portal vein (PV) systems is given by the Navier–Stokes equation

$$\rho \left( \frac{\partial \mathbf{v}}{\partial t} + \mathbf{v} \cdot \nabla \mathbf{v} \right) = -\nabla p + \mu \nabla \cdot \tau + \mathbf{b}, \quad (1)$$

where  $\rho$  is the fluid density,  $\mathbf{v} = (u, v, w)$  is the velocity vector,  $p$  is the pressure,  $\tau = \nabla \mathbf{v} + \nabla \mathbf{v}^T$  is the stress tensor,  $\mu$  is the dynamic viscosity coefficient,  $\mathbf{b}$  is the external force per unit volume and  $\nabla$  represents the gradient operator. For simplicity, we assume the blood behaves as an incompressible Newtonian fluid and the vessel walls are rigid. We also assume that there are no body forces acting on the blood flow. Besides, since the PV is far from the heart, the influence of the cardiac cycle can be neglected [6]. The momentum Eq. (1) can then be simplified into

$$-\nabla p + \mu \Delta \mathbf{v} = 0, \quad (2)$$

where  $\Delta$  is the Laplacian operator that is equal to  $\nabla \cdot \nabla$ . Since there are no sources or sinks of blood inside a vessel, the velocity field should satisfy the following continuity equation as well

$$\nabla \cdot \mathbf{v} = 0, \quad (3)$$

which indicates the blood flowing in the vessel from all inlets equals to the total amount of blood flowing out through outlets.

### 2.2 Diffuse boundary conditions

To solve Eq. (2) and (3), we propose to discretize all physical quantities on a uniform marker and cell (MAC) grid [7], as shown in Fig. 1. It is important to note that all three components of  $\mathbf{v}$  must be defined on centers of cell faces (two components in a 2D space), staggered by half a grid spacing with respect cell center on which pressure values are defined. This is to avoid non-physical wiggle solutions for the pressure and velocity fields [10]. To solve accurate hemodynamics, cells inside the vessel should be identified first. It is a common way to use a binary mask to isolate the fluid domain of interest from other tissues [9]. However, the problem with a binary threshold is that it will introduce stair-step grid artifacts into the simulation results [1].

To remove the stair-step grid artifacts, we propose to impose diffuse boundary conditions for Eq. (2) and (3). We first introduce a signed distance function

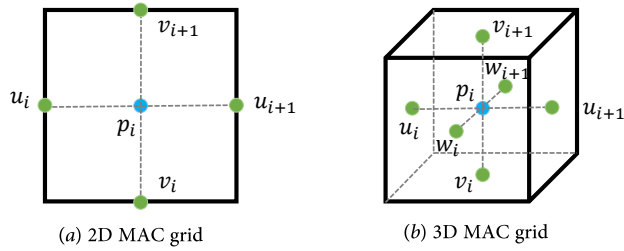


**Fig. 1.** An illustration of the MAC grid used to discretize the computational domain.

$\phi(\mathbf{x})$  to represent the blood vessel implicitly (Information on the practical implementation of how reconstruct  $\phi$  is given below under Section 2.3). For an arbitrary point  $\mathbf{x} \in \mathbb{R}^3$ ,  $|\phi(\mathbf{x})|$  tells us its distance to the vessel boundary, and  $sign(\mathbf{x}) > 0$  means  $\mathbf{x}$  is located inside a blood vessel while  $sign(\mathbf{x}) < 0$  means the opposite case. In the following discussion, we only demonstrate how to impose diffuse boundary conditions in a one-dimensional space. Consider a cell inside the vessel that is far away from the boundary (i.e.,  $u_{i+1}$ ,  $u_{i-1}$  and  $u_i$  are all located inside the computational domain), the Laplacian of  $u$  can be discretized into

$$\mathcal{L}(u_i) = \frac{u_{i+1} - 2u_i + u_{i-1}}{d^2}, \quad (4)$$

where  $d$  represents the grid spacing. Assume  $u_i$  is now located inside the boundary and  $u_{i+1}$  is located outside of the boundary, as shown in Fig. 2(a). Note

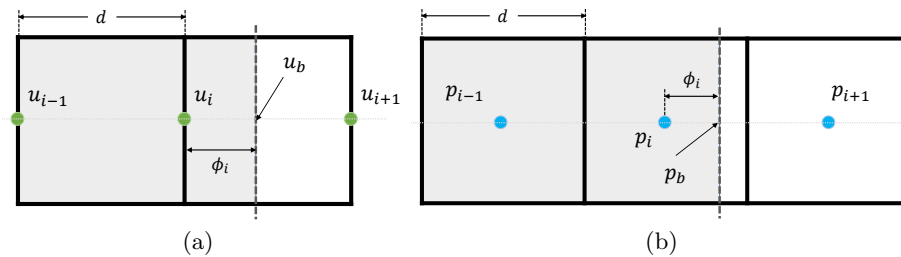


**Fig. 2.** Illustration of boundary cells. (a) velocity samples; (b) pressure samples.

that no velocity sampling point is located just on the boundary. To impose a Dirichlet velocity boundary condition of  $u_b$ , we assume  $u_{i-1}$ ,  $u_{i+1}$  and  $u_b$  satisfy the following linear relationship

$$\frac{u_b - u_{i-1}}{d + \phi_i^u} = \frac{u_{i+1} - u_b}{d - \phi_i^u}, \quad (5)$$

where  $\phi_i^u$  is the signed distance of  $u_i$ . Since  $u_{i+1}$  is outside of the boundary, we are able to reformulate  $\mathcal{L}(u_i)$  as

$$\mathcal{L}(u_i) = \frac{A_i u_b + (2 - A_i) u_{i-1} - 2u_i}{d^2}, \quad A_i = \frac{2d}{d + \phi_i^u} \quad (6)$$

after substituting Eq. 5 into Eq. 4. By clamping the value of  $\phi_i^u$  into a range of  $(0, d]$ ,  $A_i$  becomes a constant ranging from 1 to 2. Note if  $u_i$  is located on the boundary, i.e.,  $\phi_i = 0$ ,  $\mathcal{L}(u_i)$  equals to  $\frac{2u_b - 2u_i}{d^2}$ . This indicates the velocity boundary condition is directly imposed on the velocity sampling point of  $u_i$ . Otherwise, if  $\phi_i > d$ , Eq. 6 is just simplified into the form of Eq. 4 and the velocity boundary condition is imposed on the velocity sampling point  $u_{i+1}$ . In a similar way, the Laplacian of  $p$  (see an illustration in Fig 2(b)) can be formulated as

$$\mathcal{L}(p_i) = \frac{B_i p_b + (2 - B_i) p_{i-1} - 2p_i}{d^2}, \quad B_i = \frac{2d}{d + \phi_i^p} \quad (7)$$

where  $B_i$  is a constant ranging from 1 to 2, and  $\phi_i^p$  represents the clamped signed distance of  $p_i$ .

Finally, let us consider a standard discretization of the divergence of  $u$

$$\mathcal{D}(u_i) = \frac{u_{i+1} - u_i}{d}. \quad (8)$$

By imposing a Dirichlet boundary condition, we assume  $u_{i+1}$ ,  $u_i$  and  $u_b$  satisfy the following linear relationship

$$\frac{u_b - u_i}{\frac{d}{2} + \phi_i^p} = \frac{u_{i+1} - u_i}{d}, \quad (9)$$

where  $\phi_i^p$  is the signed distance of  $p_i$ . Substituting Eq. 9 into Eq. 8, the divergence of  $u$  can be reformulated as

$$\mathcal{D}(u_i) = C_i \frac{u_b - u_i}{d}, \quad C_i = \frac{2d}{d + 2\phi_i^p}, \quad (10)$$

where  $C_i$  is a constant ranging from 1 to 2 since  $\phi_i^p$  is in a range of  $[0, d/2]$ .

### 2.3 Data pre-processing and numerical implementation

To validate the proposed boundary handling technique, both model analysis and patient-specific analysis were conducted. For the patient-specific analysis, all analyses were conducted in accordance with the principles of West China Hospital and met the requirements of medical ethics. Patients' approval and informed consent were waived as our study was purely observational and retrospective in nature. All patients underwent CT angiography, and the invasive transjugular HVPG measurement. Normal subjects only underwent CT angiography. Fig. 3

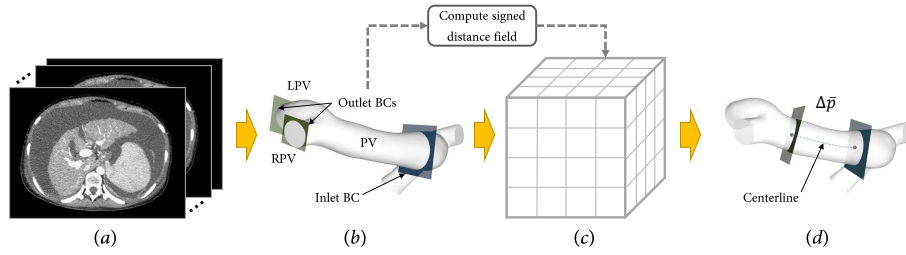


**Fig. 3.** A pipeline demonstration of all data pre-processing steps and CFD model to estimate pressure change in PV caused by blood blockage in the RPV.

outlines a pipeline showing all data-processing steps and CFD model to estimate pressure change in PV caused by blood blockage in the RPV.

*Transjugular HVPG Measurement.* The transjugular HVPG measurement (reference standard) was performed by following the established standards [3]. Pressure measurements were conducted by using a balloon catheter (Edwards Lifesciences, Irvine, California) with a pressure transducer at the tip. A zero measurement with transducer open to air was needed before the transjugular catheterization. Free hepatic venous pressure was measured in the right hepatic vein. As the balloon was inflated for total occlusion of the right hepatic vein, the wedged hepatic venous pressure was measured. Continuous recording was necessary until the pressure reached a plateau. All measurements were taken in triplicate and then averaged. HVPG was calculated by subtracting the free venous hepatic pressure from the wedged hepatic pressure.

*CT Image Acquisition.* Datas from all the subjects were collected through computed tomography systems (Sensation 64 CT (Siemens), or Sensation 16 CT (Siemens)) in West China Hospital, affiliated with Sichuan University. The triple-phase CT examinations including non-enhanced, arterial, and portal vein phase were obtained, in which portal vein phase was used to reconstruct geometric models. The scout of abdomen was acquired from the lung bases to the iliac crests including the entire liver. Arterial phase of the same region started about 20–30s after the contrast agent administration, and followed with portal venous phase (30–40s). The reconstruction was performed on advantage 3D workstation and the reconstitution thickness was set at 1–2mm.

*Segmentation of portal vein systems.* The open-source software 3D Slicer [4] was used to reconstruct the geometry of the PV system models for CFD simulation. To facilitate the hemodynamic calculations, some parts of the reconstructed surface mesh of the PV system were pruned, retaining only the PV and its main branch vessels including the left portal vein (LPV), right portal vein (RPV), superior mesenteric vein (SMV) and splenic vein (SV). Vascular centerline was extracted by the computational geometry algorithm library (CGAL) to facilitate the measurement of the distance between two probing planes (see Fig. 3(d)).

*Estimation of pressure change in PV.* Signed distance fields of blood vessels were first reconstructed with the Fast Sweeping Method [19]. Other parts were

implemented with C++ and the SIMPLE algorithm [10] was adopted to solve the discretized governing equations (2) and (3) (see supplementary materials for more details). Motivated by virtual HVPG [12], two simulations were taken for each patient-specific data. In the first simulation, Neumann velocity boundary conditions were imposed on the outlets of both LPV and RPV. In the second simulation, we virtually blocked the outlet of RPV but left LPV open to mimic a situation when patients with cirrhosis suffered from an increased resistance to blood flow through the portal system. A constant flat profile of  $\bar{u} = 0.1364m/s$  was imposed as the inlet velocity on portal vein for all models [13], including both patients and normal subjects. Finally, the pressure change before and after RPV blockage was calculated.

### 3 Experiments and Results

#### 3.1 In silico study on a steady Poiseuille flow

An analytic laminar steady flow case was first studied to verify the accuracy of our method, as sketched in Fig. 4. Since the flow is caused by a pressure gradient, the analytical solution to the Poiseuille flow in a circular pipe along axis  $x$  can be written as

$$\delta p = \frac{4\mu L u_{\max}}{R^2} \quad (11)$$

where  $\delta p$  represents the pressure drop over a length  $L$  of the pipe,  $R$  is the pipe radius and  $u_{\max}$  is the maximum velocity. Since Ansys Fluent has been commonly used to analyze hemodynamics, the steady Poiseuille flow was first solved with a finite element method embedded in ANSYS 2020 R2. To verify the accuracy under different boundary conditions, two velocity profiles were imposed at the inlet cross-sections, including a constant flat profile of  $\bar{u} = 0.2m/s$  and the corresponding exact profile  $u(r) = 2\bar{u} \left(1 - \frac{r^2}{R^2}\right) m/s$  with  $R = 5.4 \times 10^{-3}m$ . Besides, a zero-pressure boundary condition was imposed at the outlet cross-sections and a non-slip boundary condition was imposed at the vessel walls for all models. It can be noted from Fig. 4(a) that if the exact velocity profile is given, the simulation results show good convergence to the exact solution for all three different spatial resolutions. Our method does not outperform FEM at a spatial resolution of  $d = 2mm$ , but shows a good performance as the spatial resolution is increased to  $d = 0.5mm$ . Otherwise, if the constant velocity profile is given, the simulation with FEM fails to converge as grid resolution is increased, the relative error of pressure with the finest spatial resolution is still over 104%. In contrast, our method does not suffer from the sensitivity problem caused by boundary conditions and is able to reproduce consistent simulation results for both cases. This feature makes our method more applicable for further clinical applications because the exact velocity profile is usually unattainable in real situations and only an approximate average velocity can be measured (e.g., with Doppler US).

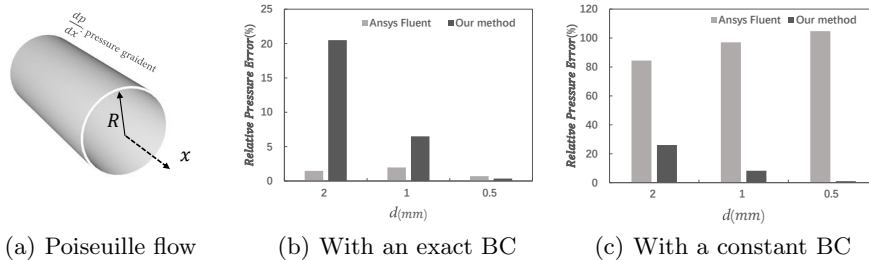


**Fig. 4.** In silico study of a steady Poiseuille flow. (a) an illustration of the steady Poiseuille flow; (b) a comparison of simulation results under an exact velocity profile; (c) a comparison of simulation results under a constant velocity profile.

### 3.2 In-vivo validation with invasive HPVPG

After in silico validation with our method, we applied it on real models constructed from CT angiographic images. We enrolled consecutive CLD patients who underwent contrast-enhanced CT within 2 weeks of HPVPG measurement. Patients were excluded according to the following criteria: (a) a prior variceal treatment (i.e., band ligation and endoscopic varices ligation (EVL)) before admission; (b) patients with histopathologically confirmed as hepatocellular carcinoma (HCC); (c) a history of splenectomy, hepatectomy or portal-azygous disconnection. A total of three patients with liver cirrhosis and three subjects with normal livers are studied. The pressure difference  $\delta p$  before and after RPV was blocked is colored mapped and demonstrated in Fig. 5. In addition, an average pressure change in PV is calculate as

$$\delta \bar{p}_{PV} = \frac{\int_{V_{PV}} \delta p dV}{l}, \quad (12)$$

where  $V_{PV}$  represents the total volume enclosed by the two probing planes as shown in Fig 3(d) and  $l$  is the length of the centerline. Note the pressure changes in PV of patients with portal hypertension (see the top row in Fig. 5) are significantly lower than that of normal subjects (see the bottom row in Fig. 5).

## 4 Conclusion

This paper proposed an Eulerian CFD model for quantifying patient-specific hemodynamics in portal vein systems non-invasively. To address boundary problems within traditional models, diffuse boundary conditions were proposed to impose smooth boundary conditions on both the pressure and velocity fields. Experiments show that our approach is less sensitive to boundary conditions and is able to reproduce consistent simulation results under two commonly used boundary conditions. The approach is also performed on patient-specific PV models reconstructed from CT angiographic images, additional experiments show that

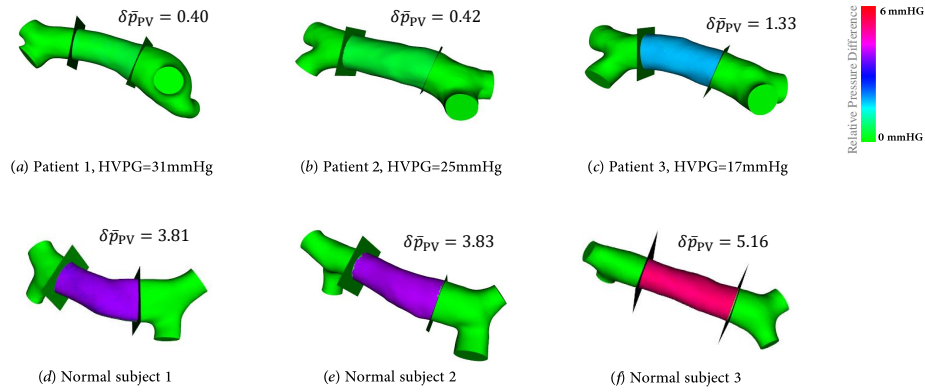


**Fig. 5.** In-vivo validation with invasive HVP. Experiments show that pressure changes in the PV of patients with portal hypertension due to blockage of the RPV is lower than that of normal subjects.

our method is able to capture pressure changes in the PV that show a significant difference between patients with portal hypertension and normal subjects.

**Acknowledgements.** This research was supported by the National Natural Science Foundation of China (No.61872345, No.62072449, No.61632003), Science and Technology Support Program of Sichuan Province(No.2021YFS0144, No.2021YFS0021), Post-Doctor Research Project, West China Hospital, Sichuan University (No.2020HXBH130), Youth Innovation Promotion Association, CAS (No.2019109).

## References

1. Batty, C., Bertails, F., Bridson, R.: A fast variational framework for accurate solid-fluid coupling. *ACM Transactions on Graphics (TOG)* **26**(3), 100–es (2007)
2. Bosch, J., Pizcueta, P., Feu, F., Fernández, M., García-Pagán, J.C.: Pathophysiology of portal hypertension. *Gastroenterology Clinics of North America* **21**(1), 1–14 (1992)
3. De Franchis, R.: Expanding consensus in portal hypertension: Report of the baveno vi consensus workshop: Stratifying risk and individualizing care for portal hypertension. *Journal of hepatology* **63**(3), 743–752 (2015)
4. Fedorov, A., Beichel, R., Kalpathy-Cramer, J., Finet, J., Fillion-Robin, J.C., Pujol, S., Bauer, C., Jennings, D., Fennessy, F., Sonka, M., et al.: 3d slicer as an image computing platform for the quantitative imaging network. *Magnetic resonance imaging* **30**(9), 1323–1341 (2012)
5. Gallo, D., De Santis, G., Negri, F., Tresoldi, D., Ponzini, R., Massai, D., Deriu, M., Segers, P., Verheghe, B., Rizzo, G., et al.: On the use of in vivo measured flow rates as boundary conditions for image-based hemodynamic models of the human aorta: implications for indicators of abnormal flow. *Annals of biomedical engineering* **40**(3), 729–741 (2012)

6. George, S., Martin, D., Giddens, D.: Portal vein contribution to the right and left lobes of the liver using mri and cfd. In: 6th World Congress of Biomechanics (WCB 2010). August 1-6, 2010 Singapore. pp. 473–476. Springer (2010)
7. Harlow, F.H., Welch, J.E.: Numerical calculation of time-dependent viscous incompressible flow of fluid with free surface. *The physics of fluids* **8**(12), 2182–2189 (1965)
8. Marfurt, K.J.: Accuracy of finite-difference and finite-element modeling of the scalar and elastic wave equations. *Geophysics* **49**(5), 533–549 (1984)
9. Marlevi, D., Ruijsink, B., Balmus, M., Dillon-Murphy, D., Fovargue, D., Pushparajah, K., Bertoglio, C., Colarieti-Tosti, M., Larsson, M., Lamata, P., et al.: Estimation of cardiovascular relative pressure using virtual work-energy. *Scientific reports* **9**(1), 1–16 (2019)
10. Patankar, S.: *Numerical heat transfer and fluid flow*. Taylor & Francis (2018)
11. Pirola, S., Cheng, Z., Jarral, O., O’Regan, D., Pepper, J., Athanasiou, T., Xu, X.: On the choice of outlet boundary conditions for patient-specific analysis of aortic flow using computational fluid dynamics. *Journal of biomechanics* **60**, 15–21 (2017)
12. Qi, X., An, W., Liu, F., Qi, R., Wang, L., Liu, Y., Liu, C., Xiang, Y., Hui, J., Liu, Z., et al.: Virtual hepatic venous pressure gradient with ct angiography (chess 1601): a prospective multicenter study for the noninvasive diagnosis of portal hypertension. *Radiology* **290**(2), 370–377 (2019)
13. QIN, Y.j., YAO, Y.z.: Characteristic of hemodynamics on liver cirrhosis resulting from chronic hepatitis b. *Journal of Pathogen Biology* **4** (2007)
14. Souguir, S.B.C., Fathallah, Raoufnand Abdallah, A.B., Hmida, B., Bedoui, M.H.: *Numerical Simulation of Venous System Blood Flow for Hepatic Donor Patient and Portal Hypertension’s Proposed Measurement*, pp. 33–38. Springer International Publishing, Cham (2020)
15. Toubia, N., Sanyal, A.J.: Portal hypertension and variceal hemorrhage. *Medical Clinics of North America* **92**(3), 551–574 (2008)
16. Vignon-Clementel, I.E., Figueroa, C.A., Jansen, K.E., Taylor, C.A.: Outflow boundary conditions for three-dimensional finite element modeling of blood flow and pressure in arteries. *Computer methods in applied mechanics and engineering* **195**(29-32), 3776–3796 (2006)
17. Yamagishi, Y., Saito, H., Tada, S., Horie, Y., Kato, S., Ishii, H., Shimojima, N., Haga, J., Shimazu, M., Kitajima, M., et al.: Value of computed tomography-derived estimated liver volume/standard liver volume ratio for predicting the prognosis of adult fulminant hepatic failure in japan. *Journal of gastroenterology and hepatology* **20**(12), 1843–1849 (2005)
18. Zhang, J.M., Zhong, L., Su, B., Wan, M., Yap, J.S., Tham, J.P., Chua, L.P., Ghista, D.N., Tan, R.S.: Perspective on cfd studies of coronary artery disease lesions and hemodynamics: a review. *International journal for numerical methods in biomedical engineering* **30**(6), 659–680 (2014)
19. Zhao, H.: A fast sweeping method for eikonal equations. *Mathematics of computation* **74**(250), 603–627 (2005)